*Materials Research*. 2015; 18(3): 473-481
DOI: http://dx.doi.org/10.1590/1516-1439.301914


# Enhanced Photocatalytic Activity of Pure Anatase $Tio_2$ and Pt-$Tio_2$ Nanoparticles Synthesized by Green Microwave Assisted Route

***Emanuela Filippo[a], Claudia Carlucci[b], Agostina Lina Capodilupo[b], Patrizia Perulli[a], Francesca Conciauro[b], Giuseppina Anna Corrente[c], Giuseppe Gigli[b,d,e], Giuseppe Ciccarella[a,b]****

[a]*Department of Innovation Engineering, University of Salento, Monteroni Street, 73100, Lecce, LE, Italy*
[b]*National Nanotechnology Laboratory – NNL, Nanoscience Institute – CNR, Arnesano Street, 73100, Lecce, LE, Italy*
[c]*University of Calabria, Pietro Bucci Street, 87036, Rende, CS, Italy*
[d]*Center for Biomolecular Nanotechnologies – CBN, Italian Institute of Technology – IIT, Barsanti Street 1, 73010, Arnesano, LE, Italy*
[e]*Department of Physics, University of Salento, Monteroni Street, 73100, Lecce, LE, Italy*

Received: June 6, 2014; Revised: March 19, 2015

High-yield, rapid and facile synthesis of elongated pure anatase titania nanoparticles has been achieved through a nonaqueous microwave-based approach. The residual organics onto nanoparticles surfaces were completely removed through a new treatment under ozone flow, at room temperature in air. Such an ozone cleaning method revealed an effective inexpensive dry process of removing organic contaminants from nanoparticles surfaces. The $TiO_2$ elongated nanoparticles having a length of $13.8 \pm 5.5$ nm and a diameter of $9.0 \pm 1.2$ nm were characterized by powder X-Ray diffraction, transmission electron microscopy, selected area diffraction, BET surface area analyzer and FT-IR spectroscopy. Photocatalytic evaluation demonstrated that the as-synthesized ozone-cleaned $TiO_2$ nanoparticles and $TiO_2$ nanoparticles loaded with platinum possess excellent Rhodamine B performance with respect to both commercial spherical nanotitania P25 and P25 loaded with platinum. This could be attributed to the anatase phase purity, small size, large specific surface area and clean surfaces of the prepared nanoparticles.

**Keywords:** *titania, microwave, nanoparticles, characterization, photocatalysis*

## 1. Introduction

Titanium dioxide ($TiO_2$) nanoparticles have been intensively studied as catalyst for the photodegradation of organic compounds due to their unique physical and chemical properties[1-3]. Their photocatalytic performance is greatly determined by the particle's crystal phase, crystallinity, phase stability, size and surface chemical properties that largely depend on their synthetic route[4]. $TiO_2$ has three nature crystallographic phases: anatase, rutile, and brookite. The physicochemical properties of the three phases are very different from each other, and they are closely related to the synthesis conditions. Anatase is the most thermodynamically stable among the three nano crystalline phases if the size of the particles is less than 11nm, brookite is the most stable phase between 11 nm and 35 nm and rutile is the most stable when all the sizes are larger than 35 nm[5]. Moreover, anatase is generally considered to be more active than rutile phase as a photocatalyst[6]. Anatase with higher crystallinity is preferred for photocatalysis, due to that the higher crystallinity offers fewer defects acting as recombination sites between photo-generated electrons and holes[7].

Many efforts have dedicated to the modification of $TiO_2$ nanoparticles in their morphology and phase structures through various methods, such as the hydrothermal synthesis method, sol–gel, anodization and template method[8]. Among these means, the hydrothermal synthesis method has received particular attention owing to its technical convenience in obtaining well-structured $TiO_2$ nanostructures. Hydrothermal synthesis, in which chemical reactions can occur in aqueous or organic media under the self-produced pressure at low temperature (usually lower than 250°C), can solve those problems encountered during sol–gel process (particles size growth, reduction of specific surface area of particles, phase transition)[9].

However, the conventional hydrothermal method usually needs high pressure and temperature, long duration and complex procedures for preparation of $TiO_2$ nanocrystals[10]. Moreover, the general synthesis of $TiO_2$ nanoparticles usually need high temperature calcinations or complex chemical processes to convert amorphous $TiO_2$ into crystallines, which generally result in grain growth of the particles and hence the loss of surface area, finally deteriorate the photocatalytic activity[11]. Thus, it would be greatly desirable to get well high yield, crystalline anatase $TiO_2$ nanoparticles in one-step synthesis procedure. The rapidly growing number of inorganic particles that were prepared by nonaqueous and/or nonhydrolytic processes clearly indicated that synthesis routes in organic

*e-mail: giuseppe.ciccarella@unisalento.it

solvents under exclusion of water represent a versatile alternative to aqueous methods[12].

More recently, microwave irradiation has been reported to effectively enhance the efficiency of hydrothermal method for the preparation of inorganic materials[13,14].

The microwave-assisted method offers a clean, cost effective, energy efficient, eco-friendly, rapid and convenient method of heating, which results in higher yields in shorter reaction times[15]. No further heat treatment is required for sample production. Microwaves are also used in synthesis to improve the nanometer size fraction of particles[16] and to enhance structural and morphological properties for the nanomaterials[17,18]. In addition, microwaves appear today as a new technology for the development of the green chemistry, with synthesis methods involving preparation procedures based on solvent-free or reduced amount of reactants[14].

Organic surfactants commonly used during synthesis process are found on the surface of the nanoparticles in trace amounts in spite of the extensive cleaning procedures to which they are subjected. Such compounds passivate the particle surface, so that nanoparticles lose their active sites and therefore affect the photocatalytic process[19].

In order to remove these substances, plasma cleaning[20], calcinations[21], super-hydride reaction[17], heat[22] and high-temperature hydrogen treatments[23] have been reported in literature. These techniques, however, either require expensive special equipment or can compromise the morphological integrity of the nanoparticles due to harsh treatment conditions. UV-ozone oxidation (UVO) is a useful alternative capable of yielding nearly atomically clean surfaces[24]. The method typically uses ultraviolet light that includes wavelengths of 185 and 257 nm, where the former generates ozone upon interacting with molecular oxygen and the latter excites the organic contaminating molecules[24]. The UV-ozone oxidation process involves the simultaneous action at room temperature of ozone and ultraviolet light, which are responsible for the oxidation of the carbon-containing compounds into carbon dioxide and water.

In this study, we developed of a rapid, non-aqueous and industrially viable relatively-low temperature synthesis method for pure anatase $TiO_2$ nanoparticles via microwave technology using Ti (IV) isopropoxide as precursor, benzyl alcohol as solvent and acetic acid as additive reagent. Furthermore, we proposed for the first time to the best of our knowledge, the use of ozone gas alone for the successful removal of the organic capping layer (acetic acid) from titania nanoparticles surface. The physicochemical characteristics of nanocrystalline ozone-treated $TiO_2$ powder in terms of morphology, crystallization, surface areas were carefully characterized.

Platinum nanoparticles were then photo-deposited onto $TiO_2$ nanoparticles and the obtained sample was labeled as Pt-$TiO_2$.

The photocatalytic activity of $TiO_2$ and Pt-$TiO_2$ samples under visible light was evaluated by degradation Rhodamine B aqueous solution as a model pollutant. A considerably enhanced photocatalytic activity was found for $TiO_2$ and Pt-$TiO_2$ nanoparticles in comparison with commercial Degussa P25 and Pt-P25, respectively, used as sample references.

## 2. Experimental Section

### *2.1. Material and methods*

Titanium (IV) isopropoxide TTIP, benzyl alcohol, acetic acid, chloroplatinic acid solution 8 wt. % in $H_2O$, Rhodamine B (purity 99%), $TiO_2$ Degussa P-25 (containing anatase and rutile phases in a ratio of about 3 : 1) were purchased from Sigma Aldrich (USA). All chemicals and solvents were of analytical grade and used without further purification. Rhodamine B consists of reddish-violet powder, its molecular formula is $C_{24}H_{31}ClN_2O_3$ (molecular weight: 479.02). Double distilled water was filtered through a Millipore membrane filter before use and used throughout the experiments.

The samples were characterized by X-ray diffraction (XRD), transmission electron microscopy (TEM), selected area diffraction pattern (SAD), BET surface area analyzer and FT-IR spectroscopy. Pt content was determined by inductively coupled plasma-atomic emission spectroscopy (ICP-AES).

X-ray diffraction measurements were carried out in the reflection mode on a Rigaku model diffractometer with Cu Kα radiation ($\lambda = 0.154$ nm). The X-ray diffraction data were collected at a scanning rate of 0.02°/s in 2θ ranging from 10° to 80°. TEM images were taken using a TEM operated at 100 kV (Jeol Jem 1011). Specimens for TEM analysis were prepared by drop-casting a single drop samples in ethanol solution onto standard carbon supported 300-mesh copper grids and drying slowly in air naturally. The nitrogen adsorption–desorption isotherms were obtained at 77 K using Brunauer–Emmett–Teller (BET) technique using a Quantachrome ASiQwin system. The FT-IR spectra of the $TiO_2$ powders were collected using a Jasco FT/IR-6300 spectrometer with a resolution of 0.07 $cm^{-1}$. UV-visible absorption spectroscopy was performed using a Varian Cary 300 Scan spectrophotometer with a 10-mm path length quartz cuvette.

### *2.2. Microwave-assisted synthesis of acetic acid capped $TiO_2$ nanoparticles*

In a typical synthesis procedure, 1ml of TTIP (3 mmol) was slowly added into 10 ml of benzyl alcohol in a vessel. Then, acetic acid (60 mmol) was added dropwise under vigorous magnetic stirring. The vessel was sealed and exposed to high intense microwave irradiation using a microwave digestion system (model Mars, CEM, Matthews, NC). The system uses a 2.45 GHz microwave frequency and it is controlled by temperature. The reaction mixture was maintained at 200°C for 45 min under medium stirring. The resulting product was collected and washed several times with methanol and finally dried under vacuum at 40°C.

### *2.3. Removal of the organic capping layer from $TiO_2$ nanoparticles.*

As a routine procedure, freshly lab-prepared colloidal nanoparticles were repeatedly washed by a large amount of solvent (methanol) and collected by centrifugation. Although excess capping agents could be stripped off from nanoparticles by extensive washing, there are always residuals resistant to removal. Generally, the presence of residual capping agents brings extra complexity to the system, such as uncertain coverage density of capping molecules and non-covalent

interaction between capping molecules and reactants, as well as charge transfer at the organic-metal interface[25]. To simplify the uncontrollable variables and to enhance their catalytic activity, nanoparticles with "clean surface" are therefore favored. We have developed a simple strategy to deal with this problem. Dried $TiO_2$ samples (200 mg) were placed in a spherical glass container with cylindrical necks and they were treated, under stirring, with an ozone ($O_3$) flow for 1 h. The ozone oxidation process involved the action of ozone alone which is responsible for the oxidation of the carbon containing compounds into carbon dioxide and water. At the same time, the oxidation products were swept off by $O_3$ gas flow. The successful removal of organic capping layer was proved through FT-IR spectroscopy.

### *2.4. Preparation of Pt loaded $TiO_2$ nanoparticles.*

The loading of Pt nanoparticles was performed on commercial P25 and ozone-treated $TiO_2$ samples. The obtained samples were labeled as Pt-P25 and Pt-$TiO_2$.

In a typical procedure, in a 100 ml beaker, titania nanoparticles (2.0 g) were dispersed in 50 ml of methanol. Then, $H_2PtCl_6$ (0.50 ml, 8 wt% aqueous solution) was added. The reaction mixture was irradiated by a 150 W Xe lamp (without an optical filter) for 30 min. The milky white suspensions turned light grayish with the deposition of Pt. The resultant Pt-titania composites were retrieved by centrifugation with 6000 rpm rotation rate, washed five times with excess methanol and dried under vacuum.

Pt contents in the catalyst were determined by ICP-AES. The catalysts were digested in aqua regia and standard solutions of known concentrations were adopted as calibration standards. ICP measurements revealed that $TiO_2$ nanoparticles were loaded with 1.0 wt% Pt metal.

### *2.5. Photodegradation of Rhodamine B*

The photocatalytic degradation of Rhodamine B was investigated in the presence of catalysts: $TiO_2$, Pt-$TiO_2$, P25 and Pt-P25. The photodegradation of Rhodamine B (RhB) for the different samples was investigated using a 150 W Xe lamp (LOT Oriel Gimbh) as source for artificial sunlight.

The catalyst sample (50 mg) was sonicated in 10 ml distilled water (15 min) to ensure complete dispersion of nanoparticles in solution. The catalyst was mixed with a $10^{-5}$ M solution of RB in distilled water (50 ml) for 30 min in the dark to reach an adsorption/desorption equilibrium. The mixture was continuously stirred in air and irradiated under Xe lamp light with a 420 nm cutoff filter to remove UV radiation. The distance between the lamp and the bottom of the solution was about 10 cm. The progress of the reaction was monitored by recording the absorption spectra of irradiated samples after every 5 min. The initial pH values of the catalyst-RhB solutions were in the range 5.2-5.8.

## 3. Results

### *3.1. Sample structural and morphological characterization*

X-ray diffraction technique was performed to analyze and identify phase formation and crystallographic information of the samples. Figure 1 shows the X-ray diffraction patterns of $TiO_2$ and P25 samples. The diffraction patterns and peak positions of $TiO_2$ nanoparticles (Figure 1a) match very well with those of tetragonal $TiO_2$ anatase with cell constants $a=b=0.37710$ nm, $c=0.9430$ nm and $\alpha=\beta=\gamma=90°$, in agreement with the standard diffraction data (JCDS 21-1272). No lines corresponding to any secondary and/or impurity phases were observed, indicating the high purity of the samples. Broad XRD peaks indicate formation of nanosized particles. XRD spectrum of the P25 (Figure 1b) confirmed the presence of anatase along with rutile phase, in agreement with the standard diffraction data (JCDS 21-1272 and 21-1276) as certified by Sigma Aldrich producer.

Transmission electron microscopy (TEM) and selected area electron diffraction pattern (SAED) have been employed to characterize the size, shape and structure of the samples. In Figure 2 a typical micrograph of the synthesized $TiO_2$ sample, with the corresponding selected area diffraction pattern is presented.

To determine the size and aspect ratio of nanomaterials, digitized TEM images obtained from randomly chosen fields, were processed with image software and the obtained data were analyzed. In such a way, more than 100 particles were analyzed. The lengths $L_A$ and widths $L_B$ were measured as the maximal length and width of the particles, respectively. The average particle length and width were $13.8 \pm 5.5$ nm and $9.0 \pm 1.2$ nm, respectively. The aspect ratio R is defined as $R=L_A/L_B$. The aspect ratio distribution reported in the inset of Figure 2a clearly evidenced that the nanoparticles have an aspect ratio in the range 1-3. The SAED pattern (Figure 2b) recorded on the area shown in Figure 2a exhibited diffraction spots/rings with interplanar spacing that could be indexed according to tetragonal $TiO_2$ anatase, as reported in Table 1. A perfect agreement in the *d* values calculated from experimental diffraction ring patterns and literature data is evident. This result confirmed the phase purity of the obtained products is high.

TEM observation of P25 sample evidenced that particles exhibited a relatively uniform particle size distribution, with an average size of about $24.1 \pm 9.5$ nm (Supplementary Information, Figure S1).

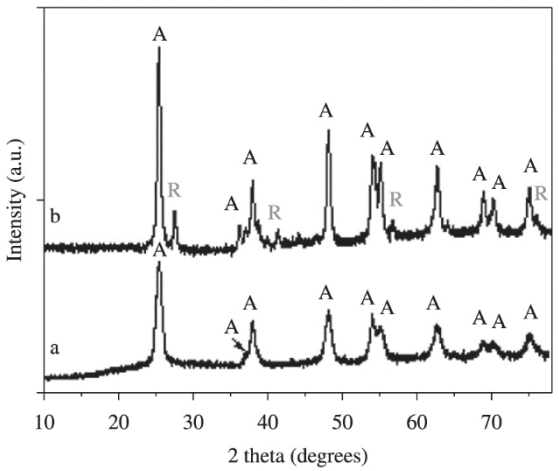


**Figure 1.** Typical XRD patterns of a) synthesized $TiO_2$ and b) P25 nanoparticles. A and R stand for anatase and rutile phase, respectively.

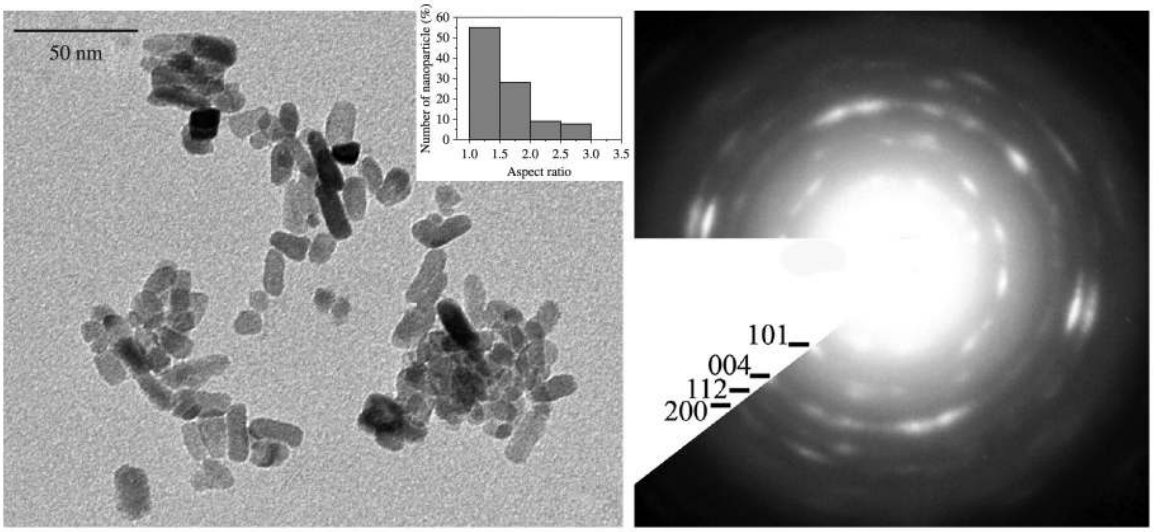


**Figure 2.** (a) Typical TEM image of the synthesized $TiO_2$ nanoparticles, with its corresponding (b) selected area diffraction pattern. Inset: aspect ratio distribution of the nanoparticles.

**Table 1.** Interplanar spacings deduced from electron diffraction pattern reported in Figure 2b together with the corresponding ones obtained from the literature data (JCPDS 21-1272).

| hkl | *d* (nm) exp. | *d* (nm) JCDS 21-1272 |
|---|---|---|
| 101 | 3.518 | 3.516 |
| 004 | 2.375 | 2.378 |
| 112 | 2.303 | 2.332 |
| 200 | 1.900 | 1.892 |

## *3.2. Removal of organic capping layer*

$TiO_2$ surface characterization was based on the FT-IR spectra (Figure 3). The as-synthesized nanoparticles (Figure 3a) have two typical absorption bands at 1451 $cm^{-1}$ and 1531 $cm^{-1}$ related to the symmetric and asymmetric stretching vibrations of the carboxylate groups. The two sharp absorption bands at 2852 $cm^{-1}$ and 2938 $cm^{-1}$ are attributed to the symmetric and asymmetric $CH_2$ stretching vibrations of molecules with long alkyl chains, respectively. The carbonyl band originating from the free ester at 1742 $cm^{-1}$ clearly shows that the non-hydrolytic sol–gel reaction of acetic acid and TTIP forms the ester[26]. Moreover, the small peaks between 3000 $cm^{-1}$ and 3100 $cm^{-1}$ can arise from the C–H stretching of the aromatic ring of benzyl alcohol, 1235 $cm^{-1}$ being typical of the C–C vibration. The treatment of the samples under ozone flow removed the organic capping layer on the surface of the nanocrystals and this phenomenon could be observed by verifying in the FT-IR spectra (Figure 3b) the disappearance of the characteristic absorption peaks at 1531 $cm^{-1}$ and 1451 $cm^{-1}$ of the chelating bidentate carboxylate groups binding to the surface of the nanocrystals[17].

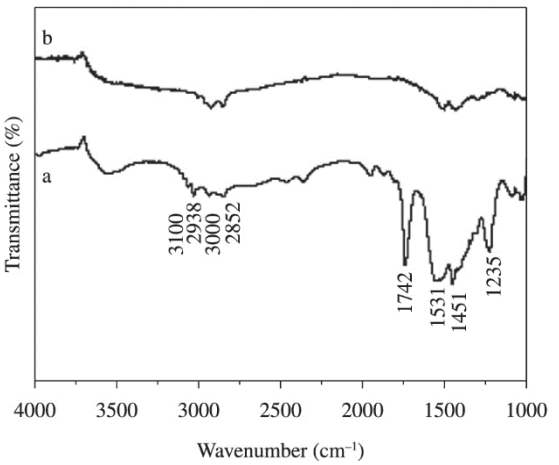


**Figure 3.** FT-IR spectra of $TiO_2$ nanoparticles a) before and b) after treatment under ozone flow for 1 h.

## *3.3. Porosity and surface area characterization*

The structural and textural properties of the ozone-treated $TiO_2$ samples were investigated by $N_2$ adsorption–desorption isotherms at 77 K. Figure 4 shows the obtained results

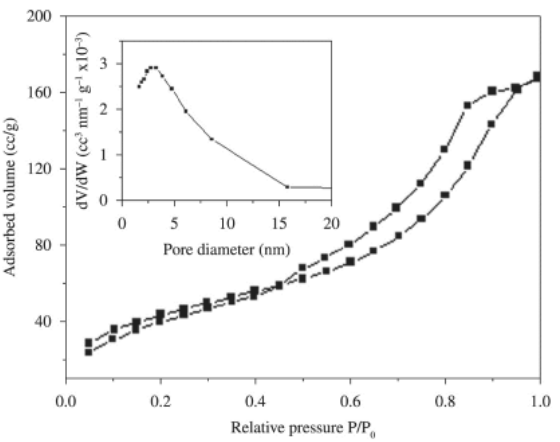


**Figure 4.** Nitrogen adsorption-desorption and pore size distribution (inset) of ozone treated $TiO_2$ nanoparticles.

analyzed by BET method for surface area and BJH pore size distribution as inset. The relative isotherm of the sample was of type IV, which is characteristic of mesoporous materials. The Brunauer–Emmett–Teller (BET) specific surface area analysis result was 89.46 $m^2\ g^{-1}$, denoting a significant increase of the surface area compared to P25 (56 $m^2\ g^{-1}$). The BJH pore size distributions (inset of Figure 4) evidenced an average pore diameter of about 2.9 nm.

The obtained high and uniform porosity could ensure enhanced reaction rates due to the high level of interaction of the reactants with the active sites.

### *3.4. Pt loading onto $TiO_2$ nanoparticles*

XRD spectrum acquired after Pt photodeposition didn't show any difference with respect to un-loaded sample. When the impurity level onto the surface of any sample, Pt in this case, remains less than 5%, it is less likely to be detected by XRD but the presence of Pt onto the surface of $TiO_2$ was confirmed by TEM, EDX and ICP analysis (Supplementary Information, Figure S2).

TEM observations of platinum loaded sample (Figure 5) evidenced that the estimated range of Pt nanoparticles deposited onto the surface of $TiO_2$ nanoparticles was found to be 1-2 nm. Small black dots in TEM images are platinum particles.

It is well known that there is no chemical bonding between Pt and $TiO_2$ surface, but Pt remains adhered onto the oxide surface by a well known interaction called strong metal (Pt)-support ($TiO_2$) interaction (SMSI)[27]. The photodeposition of platinum nanoparticles was carried out in acidic environment in order to avoid possible agglomeration of platinum. In fact, in acidic environment the titania particles surface is positively charged, since zero point of charge ($pH_{zpc}$) is at a pH of 6.25. The positively charged $TiO_2$ surface will facilitate adsorption of $PtCl^{2-}_6$ and its hydrolyzed ions (the concentration of anions will be higher on the surface), thereby increasing the entrapment of excited conduction band electrons resulting in a high deposition rate of platinum nanoparticles on the support[28].

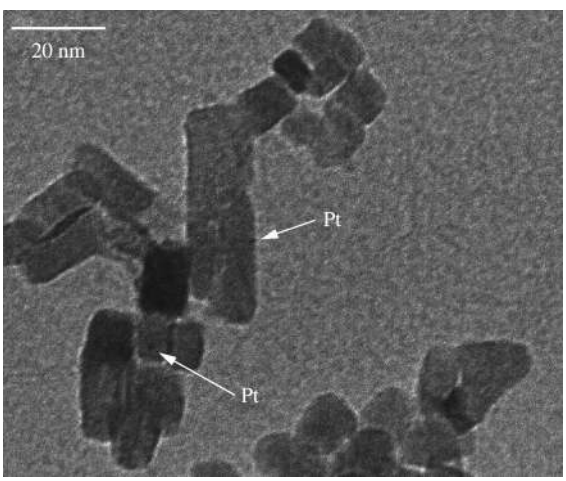


**Figure 5.** Typical TEM image of Pt loaded $TiO_2$ nanoparticles.

### *3.5. Formation of anatase nanoparticles.*

$TiO_2$ nanoparticles synthesis method presented in this work is based on a microwave-assisted non-aqueous sol-gel process, where titanium tetraisopropoxide is used as titanium oxide precursor, benzyl alcohol as solvent and acetic acid as additive reagent. Benzyl alcohol is a mildly coordinating solvent, with a high boiling point, benign in nature and several reports have documented the non-aqueous synthesis of monodisperse and well separated $TiO_2$ nanoparticles, where benzyl alcohol has been employed as a solvent. Niederberger et al. [29] found that the reaction between benzyl alcohol and $TiCl_4$ could provide a versatile method for non-aqueous preparation of $TiO_2$ nanocrystals: 5 nm sized anatase nanoparticles were obtained by means of a synthesis performed at 40 °C for 7-14 days[29]. Melcarne et al.[30] and Zimmermann et al.[31] proposed a modification of this non-aqueous sol-gel process by the use of TTIP as titanium oxide precursor. However, the proposed synthetic approach required still long reaction time (12 h and 48 h, respectively). In our microwave-assisted synthetic approach, microwave irradiation with respect to conventional heating greatly accelerates nanoparticle formation by facilitating the dissolution of the precursor in the solvent and increasing the rate constants for the esterification reaction, resulting in faster production of monomer and consequently in an earlier nucleation event[32]. Moreover, acetic acid further catalyses crystallization, and due to the fast nucleation and slow growth and coarsening kinetics, the number of particles is large[33], thus limiting the particle radius to about 10-15 nm.

It is well known that anatase is formed due to the lower surface energy as compared to the other phases. The lower surface energy affects phase formation in terms of thermodynamics and kinetics. Thermodynamically, anatase is the structure with the lowest total energy if the nanoparticles are sufficiently small[34].

It has been remarked that this method does not require water as solvent because the esterification reaction between the benzyl alcohol and the unreacted acetic acid gradually provides water into the reaction environment[30]. It constitutes, then, a simple and fast procedure for the preparation of uniform size $TiO_2$ anatase nanoparticles. It is particularly fit to be scaled-up on large volumes in the perspective of a potential industrialization.

### *3.6. Photocatalytic degradation of Rhodamine B by $TiO_2$, P25, Pt-$TiO_2$ and Pt-P25 samples.*

Photocatalytic degradation of Rhodamine B (RhB) was evaluated using $TiO_2$, P25, Pt-$TiO_2$ and Pt-P25 samples in suspensions. All experiments were conducted at the natural pH of the dye.

Blank experiments were carried out on a RhB solution containing no catalyst and they proved the occurrence of negligible degradation of the dye upon direct visible photolysis. This may be due to the natural self-fading of the dye. In addition, RhB-titania samples kept in the dark didn't show any appreciable absorbance changes over time.

The variation of concentration of RhB in $TiO_2$ and Pt-$TiO_2$ catalyzed systems as function of time was evaluated and compared with P25 and Pt-P25. It was evident that UV-Vis characteristic absorption peak at 554 nm of the

RhB solution gradually decreases during illumination time for all samples (Supplementary Information, Figure S3). The possible photodegradation of RhB includes four main processes: N-deethylation, chromophore cleavage, ring opening and mineralization.

The curves of changes in relative concentration of RhB (calculated from the absorption at 554 nm) versus irradiation time for each sample are demonstrated in Figure 6a.

It is clear that our $TiO_2$ nanoparticles sample shows significant improvement in the photodegradation of RhB compared to P25 and also to Pt-P25. The degradation is fastest and the concentration follows an exponential decay. It can be seen that RhB solution was almost degraded completely within 20 min using Pt-$TiO_2$, within 40 min using $TiO_2$ samples. Comparing the synthesized samples with the reference ones (P25and Pt-P25), the degradation process slows down significantly at longer reaction times.

According to numerous literature works, the influence of the initial concentration of the solute on the photocatalytic degradation rate of the most organic compounds is described by pseudo-first order kinetics[35]

$$-\frac{dC}{dt} = kC \quad (1)$$

where k ($min^{-1}$) is the apparent rate constant and is affected by dyes stuff concentration. Integration of Equation 1 will lead to the expected relation

$$\ln\left(\frac{C_0}{C}\right) = kt. \quad (2)$$

The plot of Equation 2 versus *t* for the different studied catalyst is shown in Figure 6b. The figure shows that the photocatalytic degradation follows the pseudo-first order. The apparent rate constants for all studied samples is determined from the slopes of $\ln(C_0/C)$ *versus* irradiation time and the obtained values with the corresponding standard error (SE) are summarized in Table 2.

Remarkably, the reaction rate constant of $TiO_2$ and Pt-$TiO_2$ samples are about 8 and 6 times, respectively as high as those of commercial P25 and Pt-P25.

The enhanced photocatalytic activity of prepared $TiO_2$ sample with respect to P25 can be attributed the larger BET surface area, which can offer more active adsorption sites and photocatalytic reaction centers and to the presence of only pure anatase phase, which is known to be more active than rutile phase for $TiO_2$ photocatalyst.

The enhancement in decomposition rate of organic pollutants in the presence of metalized $TiO_2$ has been discussed previously by several authors. The enhancement in decomposition rate of organic pollutant in the presence of metalized metal oxides may be mainly attributed to the formation of a Schottky barrier between the metal and the semiconductor[36]. So, when the platinum particles are deposited onto the surface of $TiO_2$, a Schottky barrier formed at the interface of $TiO_2$ and Pt metal particles, resulting in an efficient channeling of excited conduction band electrons from the bulk of $TiO_2$ to the newly formed interface. As a result, the electron density in $TiO_2$ particles decreases which in turn prevents the electron–hole pair recombination. As a result, higher photocatalytic activity was observed.

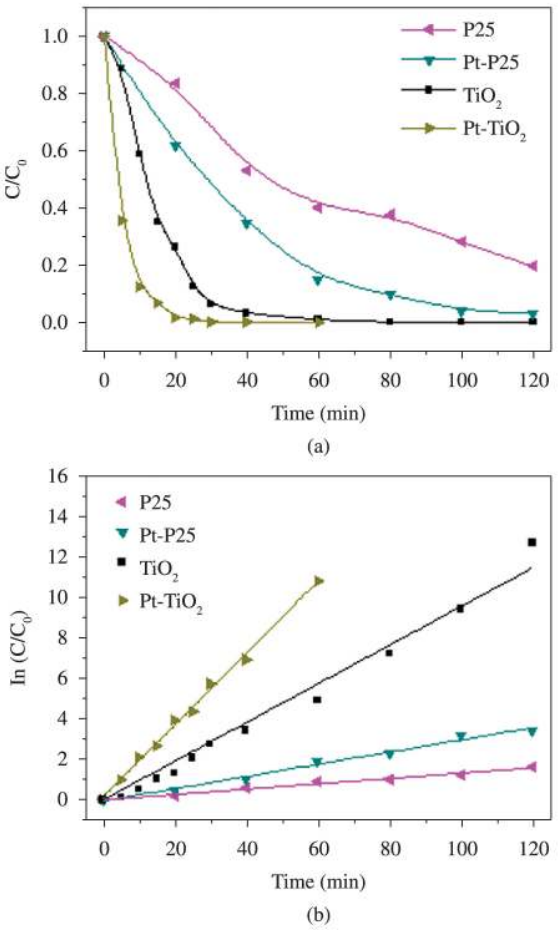


**Figure 6.** a) Photocatatalytic degradation of RhB solution by synthesized $TiO_2$ and Pt-$TiO_2$ and reference P25 and Pt-P25 samples under visible light irradiation; b) first order kinetic plot for the photodegradation of RhB

**Table 2.** Apparent rate constant *k* values for the different samples.

| Sample ($\times 10^{-3}$ $min^{-1}$) | P25 | Pt-P25 | $TiO_2$ | Pt-$TiO_2$ |
|---|---|---|---|---|
| k | 13 | 30 | 102 | 178 |
| SE | 1 | 2 | 3 | 4 |

## 4. Conclusion

A facile and rapid synthesis of phase-pure anatase $TiO_2$ nanoparticles through a nonaqueous microwave assisted process has been reported, using Ti(IV) isopropoxide as precursor, benzyl alcohol as solvent and acetic acid as additive reagent. Slightly elongated nanoparticles with a length of 13.8 ± 5.5 nm and a diameter of 9.0 ±1.2 nm were obtained after a reaction period of 45 min.

Since capping agents bring extra complexities for the catalytic study of colloidal nanoparticles, in order to simplify the uncontrollable variables and to enhance nanoparticles catalytic activity, the residual organics onto nanoparticles surfaces were completely removed through a new low-cost treatment under ozone flow, at room temperature in air.

The successful removal of organic capping layer has been proved through FT-IR spectroscopy.

Experimental results evidenced that synthesized anatase titania nanoparticles exhibited higher photocatalytic activity compared to P25 and Pt-P25. Moreover, the photocatalytic activity of the synthesized nanoparticles was further increased by Pt loading. The improved photocatalytic performance could be attributed to the anatase phase purity, small size, large specific surface area and clean surfaces of the prepared nanoparticles. In fact, anatase is generally considered to be more active than rutile phase for $TiO_2$ photocatalyst. The larger surface area of $TiO_2$ nanoparticles with cleaned surfaces is beneficial for the RhB adsorption, further leading to more photoexcited electrons transferred from RhB to $TiO_2$ and accompanied with higher dye degradation efficiency.

## Acknowledgements

This research was supported by PON 254/Ric. Potenziamento del "CENTRO RICERCHE PER LA SALUTE DELL'UOMO E DELL'AMBIENTE" Cod. PONa3_00334, PON Avviso prot. n. 84/Ric., NAnoMAteriali per l'edilizia SosTEnibile (NAMASTE) prot. PON04a3_00107 –Regione Puglia Aiuti e sostegno dei partenariati regionali per l'innovazione Nano/Micro Strutturazione nei materiali per l'Edilizia ed altri settori produttivi (NAMISTE) Cod. 2Y6DME5 and the FIRB 2009/2010 project "Rete integrata per la Nano Medicina (RINAME)" – RBAP114AMK_006.

## References

1. Kamat PV. Photophysical, photochemical and photocatalytic aspects of metal nanoparticles. *The Journal of Physical Chemistry B*. 2002; 106(32):7729-7744. http://dx.doi.org/10.1021/jp0209289.
2. Subramanian V, Wolf E and Kamat PV. Semiconductor-metal composite nanostructures. To what extent do metal nanoparticles improve the photocatalytic activity of TiO2 films. *The Journal of Physical Chemistry B*. 2001; 105(46):11439-11446. http://dx.doi.org/10.1021/jp011118k.
3. Cho Y, Choi W, Lee CH, Hyeon T and Lee HI. Visible light-induced degradation of carbon tetrachloride on dye-sensitized TiO2. *Environmental Science & Technology*. 2001; 35(5):966-970. http://dx.doi.org/10.1021/es001245e. PMid:11351543
4. Macwan DP, Dave PN and Chaturvedi S. A Review on nano TiO2 sol-gel type synthesis and its application. *Journal of Materials Science*. 2011; 46(11):3669-3686. http://dx.doi.org/10.1007/s10853-011-5378-y.
5. Wei X, Zhu G, Fan J and Chen J. Synthesis, characterization and photocatalysis of well-dispersible phase-pure anatase TiO2 nanoparticles. *International Journal of Photoenergy*. 2013; 2013:726872.
6. Hurum DC, Agrios AG, Gray AK, Rajh T and Thurnauer MC. Explaining the enhanced photocatalytic activity of Degussa P25 mixed phase TiO2 using EPR. *The Journal of Physical Chemistry B*. 2003; 107(19):4545-4549. http://dx.doi.org/10.1021/jp0273934.
7. He D and Lin F. Preparation and photocatalytic activity of anatase TiO2 nanocrystallites with high thermal stability. *Materials Letters*. 2007; 61(16):3385-3387. http://dx.doi.org/10.1016/j.matlet.2006.11.075.
8. Yu X, Li Y, Wlodarski W, Kandasamy S and Kalantarzadeh K. Fabrication of nanostructured TiO2 by anodization: a comparison between electrolytes and substrates. *Sensors and Actuators. B, Chemical*. 2008; 130(1):25-31. http://dx.doi.org/10.1016/j.snb.2007.07.076.
9. Kim C-S, Moon BK, Park J-H, Chung ST and Son S-M. Synthesis of nanocrystalline TiO2 in toluene by a solvothermal route. *Journal of Crystal Growth*. 2003; 254(3-4):405-410. http://dx.doi.org/10.1016/S0022-0248(03)01185-0.
10. Ito S, Murakami TN, Comte P, Liska P, Gratzel C, Nazeeruddin MK, et al. Fabrication of thin film dye sensitized solar cells with solar to electric power conversion efficiency over 10%. *Thin Solid Films*. 2008; 516(14):4613-4619. http://dx.doi.org/10.1016/j.tsf.2007.05.090.
11. Jing J, Feng J, Li W and Yu WW. Low-temperature synthesis of water-dispersible anatase titanium dioxide nanoparticles for photocatalysis. *Journal of Colloid and Interface Science*. 2013; 396:90-94. http://dx.doi.org/10.1016/j.jcis.2012.12.075. PMid:23407148
12. Pinna N and Niederberger M. Surfactant-free nonaqueous synthesis of metal oxide nanostructures. *Angewandte Chemie International Edition*. 2008; 47(29):5292-5304. http://dx.doi.org/10.1002/anie.200704541. PMid:18561355
13. Zhang P, Yin S and Sato T. Synthesis of high-activity TiO2 photocatalyst via environmentally friendly and novel microwave assisted hydrothermal process. *Applied Catalysis B: Environmental*. 2009; 89(1-2):118-122. http://dx.doi.org/10.1016/j.apcatb.2008.12.002.
14. Huang CH, Yang YT and Doong RA. Microwave assisted hydrothermal synthesis of mesoporous anatase TiO2 via sol-gel process for dye-sensitized solar cells. *Microporous and Mesoporous Materials*. 2011; 142(2-3):473-480. http://dx.doi.org/10.1016/j.micromeso.2010.12.038.
15. Monti D, Ponrouch A, Estruga M, Palacin MR, Ayllon JA and Roig A. Microwaves as a synthetic route for preparing electrochemically active TiO2 nanoparticles. *Journal of Materials Research*. 2013; 28(3):28340-28347.
16. Lagashetty A, Havanoor V, Basavaraja S, Balaji SD and Venkataraman A. Microwave assisted route for synthesis of nanosized metal oxide. *Science and Technology of Advanced Materials*. 2007; 8(6):484-493. http://dx.doi.org/10.1016/j.stam.2007.07.001.
17. Carlucci C, Xu H, Scremin BF, Giannini C, Altamura D, Carlino E, et al. Selective synthesis of TiO2 nanocrystals with morphology control with the microwave-solvothermal method. *CrystEngComm*. 2014; 16(9):1817-1824. http://dx.doi.org/10.1039/c3ce41477a.
18. Xu H, Carlucci C, Scremin BF, Giannini C, Sibillano T, Scrascia A, et al. Synthesis of ultrafine anatase titanium dioxide (TiO2) nanocrystals by the microwave-solvothermal method. *Journal of Nanoengineering and Nanomanufacturing*. 2014; 4(1):28-32. http://dx.doi.org/10.1166/jnan.2014.1165.
19. Thompson TL and Yates JT Jr. Surface science studies of the photoactivation of TiO2—new photochemical processes. *Chemical Reviews*. 2006; 106(10):4428-4453. http://dx.doi.org/10.1021/cr050172k. PMid:17031993
20. Gehl B, Fromsdorf A, Aleksandrovic V, Schmidt T, Pretorius A, Flege JI, et al. Structural and chemical effects of plasma

treatment on close-packed colloidal nanoparticle layers. *Advanced Functional Materials*. 2008; 18(16):2398-2410. http://dx.doi.org/10.1002/adfm.200800274.

21. Lange C, De Caro D, Gamez A, Storck S, Bradley JS and Maier WF. Polymer induced selectivity enhancement in the hydrogenation of 2-hexyne catalyzed by poly(vinylpyrrolidone)-stabilized platinum colloids in an amorphous mixed metal oxide support. *Langmuir*. 1999; 15(16):5333-5338. http://dx.doi.org/10.1021/la981708i.
22. Wang ZL, Petroski JM, Green TC and El-Sayed MA. Shape transformation and surface melting of cubic and tetrahedral platinum nanocrystals. *The Journal of Physical Chemistry B*. 1998; 102(32):6145-6151. http://dx.doi.org/10.1021/jp981594j.
23. Lee I, Morales R, Albiter MA and Zaera F. Synthesis of heterogeneous catalysts with well shaped platinum particles to control reaction selectivity. *Proceedings of the National Academy of Sciences of the United States of America*. 2008; 105(40):15241-15246. http://dx.doi.org/10.1073/pnas.0805691105. PMid:18832170
24. Vig JR. UV/ozone cleaning of surfaces. *Journal of Vacuum Science & Technology. A, Vacuum, Surfaces, and Films*. 1985; 3(3):1027-1034. http://dx.doi.org/10.1116/1.573115.
25. Niu Z and Li Y. Removal and utilization of capping agents in nanocatalysis. *Chemistry of Materials*. 2014; 26(1):72-83. http://dx.doi.org/10.1021/cm4022479.
26. Joo J, Kwon SG, Yu T, Cho M, Lee J, Yoon J, et al. Large-scale synthesis of TiO2 nanorods via nonhydrolytic sol-gel ester elimination reaction and their application to photocatalytic inactivation of E. coli. *The Journal of Physical Chemistry B*. 2005; 109(32):15297-15302. http://dx.doi.org/10.1021/jp052458z. PMid:16852938
27. Lewera A, Timperman L, Roguska A and Alonso-Vante NA. Metal-support interactions between nanosized Pt and metal oxides (WO3 and TiO2) studied using X-ray photoelectron spectroscopy. *The Journal of Physical Chemistry C*. 2011; 115(41):20153-20159. http://dx.doi.org/10.1021/jp2068446.
28. Muneer M, Qamar M, Saquib M and Bahnemann DW. Heterogeneous photocatalysed reaction of three selected pesticide derivatives, propham, propachlor and tebuthiuron in aqueous suspensions of titanium dioxide. *Chemosphere*. 2005; 61(4):457-468. http://dx.doi.org/10.1016/j.chemosphere.2005.03.006. PMid:16202799
29. Niederberger M, Bartl MH and Stucky GD. Benzyl alcohol and titanium tetrachloride: a versatile reaction system for the nonaqueous and low-temperature preparation of crystalline and luminescent titania nanoparticles. *Chemistry of Materials*. 2002; 14(10):4364-4370. http://dx.doi.org/10.1021/cm021203k.
30. Melcarne G, De Marco L, Carlino E, Martina F, Manca M, Cingolani R, et al. Surfactant-free synthesis of pure anatase TiO2 nanorods suitable for dye-sensitized solar cells. *Journal of Materials Chemistry*. 2010; 20(34):7248-7254. http://dx.doi.org/10.1039/c0jm01167c.
31. Zimmermann M and Garnweitner G. Spontaneous water release inducing nucleation during the nonaqueous synthesis of TiO2 nanoparticles. *CrystEngComm*. 2012; 14(24):8562-8568. http://dx.doi.org/10.1039/c2ce25934f.
32. Bilecka I, Elser P and Niederberger M. Kinetic and thermodynamic aspects in the microwave-assisted synthesis of ZnO nanoparticles in benzyl alcohol. *ACS Nano*. 2009; 3(2):467-477. http://dx.doi.org/10.1021/nn800842b. PMid:19236087
33. Coronado DR, Gattorno GR, Espinosa Pesqueira ME, Cab C, Coss R and Oskam G. Phase pure TiO2 nanoparticles: anatase, brookite and rutile. *Nanotechnology.* 2008;19(14):145605.
34. Oskam G. Metal oxide nanoparticles: synthesis, characterization and application. *Journal of Sol-Gel Science and Technology*. 2006; 37(3):161-164. http://dx.doi.org/10.1007/s10971-005-6621-2.
35. Barka N, Qourzal S, Assabbane A, Nounah A and Ait-Ichou Y. Factors influencing the photocatalytic degradation of Rhodamine B by TiO2 coated non-woven paper. *Journal of Photochemistry and Photobiology A Chemistry*. 2008; 195(2-3):346-351. http://dx.doi.org/10.1016/j.jphotochem.2007.10.022.
36. Hufschmidt D, Bahnemann D, Testa JJ, Emilio CA and Litter MI. Enhancement of the photocatalytic activity of various TiO2 materials by platinisation. *Journal of Photochemistry and Photobiology A Chemistry*. 2002; 148(1-3):223-231. http://dx.doi.org/10.1016/S1010-6030(02)00048-5.

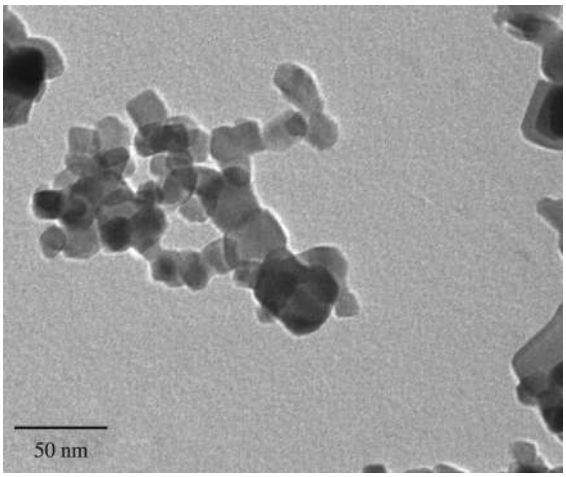


**Figure S1.** Typical TEM image of P25 nanoparticles.

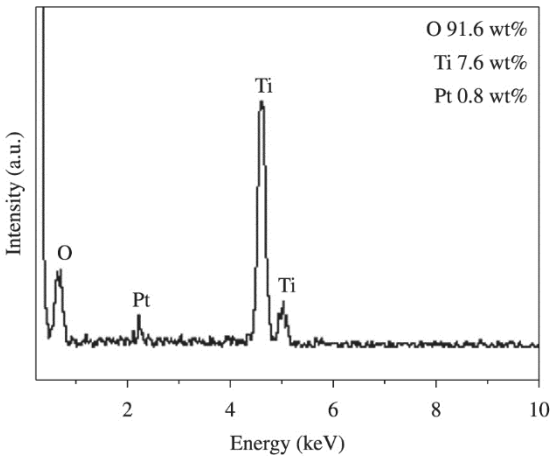


**Figure S2.** Typical EDX spectrum acquired from Pt-$TiO_2$ sample.

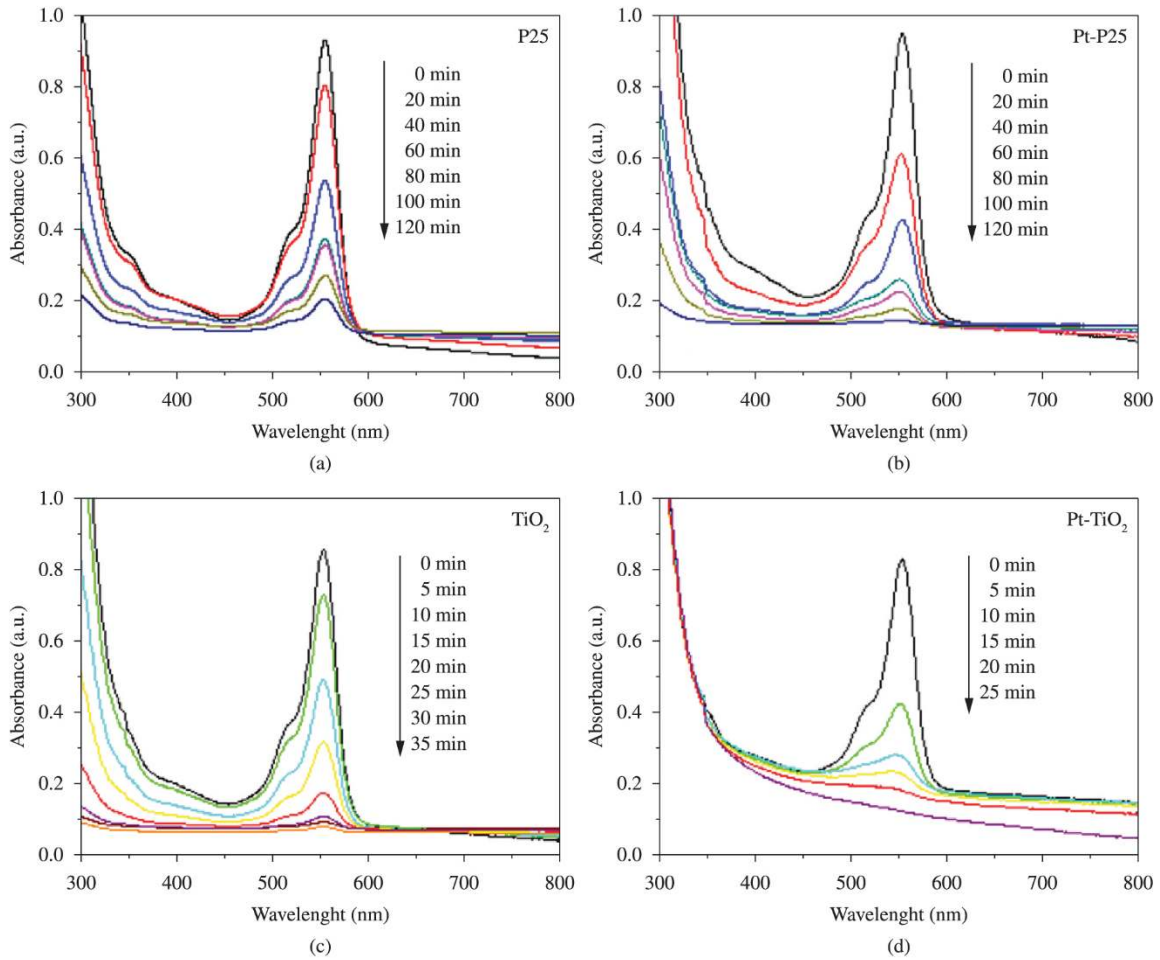


**Figure S3.** Change of the characteristic absorbance intensity of the RhB solution (at 554 nm) as a function of irradiation time for a) P25, b) Pt-P25, c) $TiO_2$ and d) Pt-$TiO_2$ samples.